The Pacific Meridional Mode and the Occurrence of Tropical Cyclones in the Western North Pacific

W. ZHANG

Key Laboratory of Meteorological Disaster, Ministry of Education, Collaborative Innovation Center on Forecast and Evaluation of Meteorological Disasters, and Earth System Modeling Center, Nanjing International Academy of Meteorological Sciences, Nanjing University of Information Science and Technology, Nanjing, China, and NOAA/Geophysical Fluid Dynamics Laboratory, and Atmospheric Oceanic Sciences Program, Princeton University, Princeton, New Jersey

G. A. VECCHI AND H. MURAKAMI

NOAA/Geophysical Fluid Dynamics Laboratory, and Atmospheric and Oceanic Sciences Program, Princeton University, Princeton, New Jersey

G. VILLARINI

IIHR-Hydroscience and Engineering, The University of Iowa, Iowa City, Iowa

L. JIA

NOAA/Geophysical Fluid Dynamics Laboratory, and Atmospheric and Oceanic Sciences Program, Princeton University, Princeton, New Jersey

(Manuscript received 21 April 2015, in final form 25 August 2015)

ABSTRACT

This study investigates the association between the Pacific meridional mode (PMM) and tropical cyclone (TC) activity in the western North Pacific (WNP). It is found that the positive PMM phase favors the occurrence of TCs in the WNP while the negative PMM phase inhibits the occurrence of TCs there. Observed relationships are consistent with those from a long-term preindustrial control experiment (1000 yr) of a high-resolution TC-resolving Geophysical Fluid Dynamics Laboratory (GFDL) Forecast-Oriented Low Ocean Resolution (FLOR) coupled climate model. The diagnostic relationship between the PMM and TCs in observations and the model is further supported by sensitivity experiments with FLOR. The modulation of TC genesis by the PMM is primarily through the anomalous zonal vertical wind shear (ZVWS) changes in the WNP, especially in the southeastern WNP. The anomalous ZVWS can be attributed to the responses of the atmosphere to the anomalous warming in the northwestern part of the PMM pattern during the positive PMM phase, which resembles a classic Matsuno–Gill pattern. Such influences on TC genesis are strengthened by a cyclonic flow over the WNP. The significant relationship between TCs and the PMM identified here may provide a useful reference for seasonal forecasting of TCs and interpreting changes in TC activity in the WNP.

1. Introduction

Tropical cyclones (TCs) are among the most destructive and costly natural disasters on Earth (e.g., Rappaport 2000; Pielke et al. 2008; Q. Zhang et al. 2009). The occurrence of TCs has long been the subject of scientific inquiry (e.g., Mitchell 1932; Gray 1968; Henderson-Sellers et al. 1998; Simpson et al. 1998; Vitart and Stockdale 2001; Liu and Chan 2003; Klotzback 2007; Chan 2008a,b; Sippel and Zhang 2008; Lin et al. 2014; Vecchi et al. 2014). Large-scale climate variations in various basins affect the occurrence of TCs in the western North Pacific (WNP) by both local and remote forcing. In general, variations in TC occurrence in the WNP are closely associated with the sea surface temperature (SST) patterns such as El Niño–Southern Oscillation (ENSO) (Chan 1985; Wu and Lau 1992; Chan 2000; Wang and Chan 2002; Camargo and Sobel 2005; Zhang

Corresponding author address: Wei Zhang, National Oceanic and Atmospheric Administration/Geophysical Fluid Dynamics Laboratory, 201 Forrestal Road, Princeton, NJ 08540.
E-mail: wei.zhang@noaa.gov

DOI: 10.1175/JCLI-D-15-0282.1

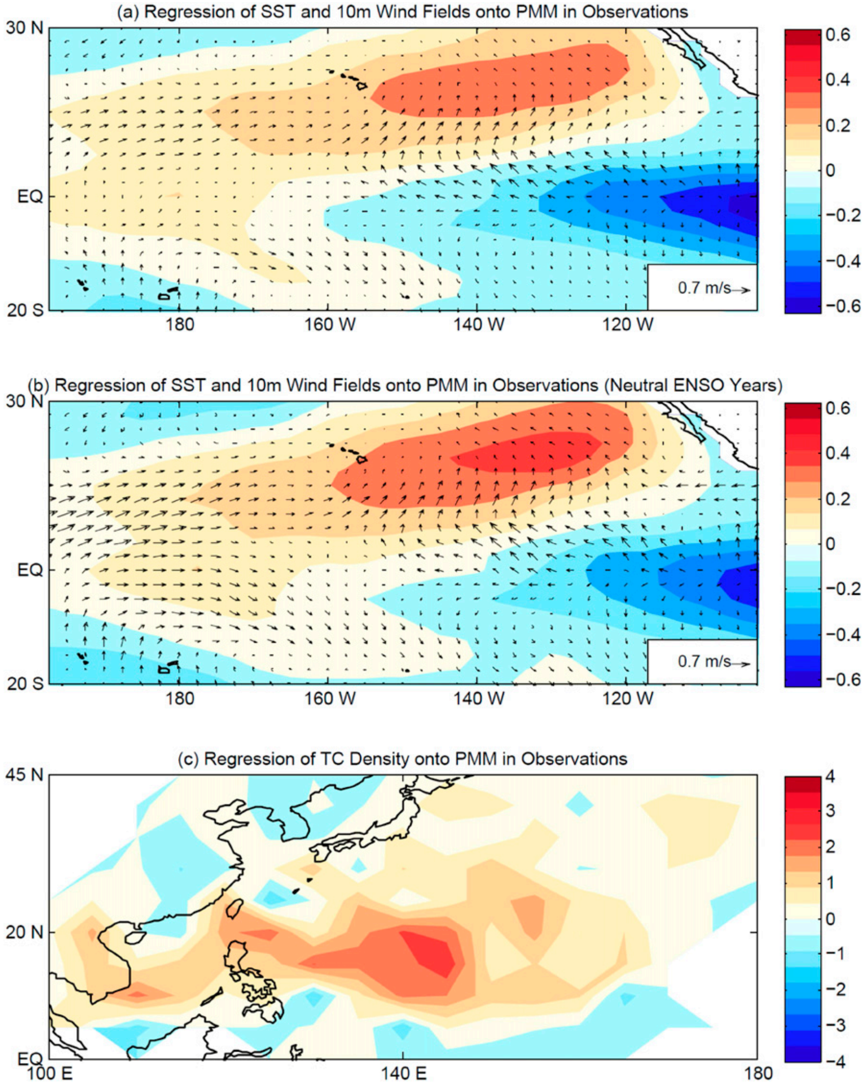

FIG. 1. The regression of SST (°C) and 10-m wind fields (ms^{-1}) during (a) 1961–2013, (b) neutral ENSO years during 1961–2013, and (c) tropical cyclone track density onto the standardized PMM index. The spatial domains in (a) and (b) are consistent with that in Chiang and Vimont (2004).

et al. 2012), the Indian Ocean warming (Du et al. 2011; Zhan et al. 2011, 2014), the North Pacific Gyre Oscillation (Zhang et al. 2013), and the Pacific decadal oscillation (PDO) (Lee et al. 2012; Liu and Chan 2013; Girishkumar et al. 2014). Recently it has been suggested that the SST in the North Atlantic also modulates TC activity in the WNP (Li et al. 2013; Huo et al. 2015).

The Pacific meridional mode (PMM) is defined here as the first maximum covariance analysis (MCA) mode of SST and 10-m wind vectors in the Pacific Ocean, and describes meridional variations in SST, winds, and convection in the tropical Pacific (Chiang and Vimont 2004). The PMM (refer to Fig. 1a) bears marked resemblance to the Atlantic meridional mode (AMM) in terms of its principal mechanisms, impacts, and interactions with extratropical climate systems (Chiang and Vimont 2004). For example, the North Pacific Oscillation (NPO) has been found to force the PMM, while the North Atlantic Oscillation (NAO) acts to force the AMM (Vimont et al. 2003).

The PMM is closely associated with ENSO (Chang et al. 2007; Alexander et al. 2008; L. Zhang et al. 2009; Larson and Kirtman 2013; Lin et al. 2015), with the PMM peaking around April and May, whereas ENSO usually reaches its peak during the boreal winter (Chang et al. 2007; L. Zhang et al. 2009; Larson and Kirtman 2013; Lin et al. 2015). Previous studies have indicated that the PMM may set the stage for the seasonal peak of ENSO (Larson and Kirtman 2014). However, the PMM can also exist independently of ENSO, with the ENSO effect routinely removed through linear regression onto the cold tongue index (CTI) when calculating the PMM index (Chiang and Vimont 2004; L. Zhang et al. 2009; Larson and Kirtman 2014).

Previous research has found that the seasonal occurrence and accumulated energy of hurricanes in the North Atlantic are strongly influenced by the AMM (Vimont and Kossin 2007; Smirnov and Vimont 2011). More recently, Patricola et al. (2014) examined the combined influence of the AMM and ENSO on hurricane activity in the North Atlantic; they found that hurricane activity is profoundly enhanced when the positive AMM phase and La Niña overlap. Basically, the PMM pattern consists of two parts: a northwestern part from the North America coast toward Hawaii and a southeastern part in the eastern Pacific (Chiang and Vimont 2004; see Fig. 1a). During the positive PMM phase, positive SST anomalies prevail in the northwestern part while negative SST anomalies prevail in the southeastern part (Chiang and Vimont 2004). Such SST anomalies can be hypothesized to affect TC activity in the WNP by modulating the large-scale circulation, much like the PMM has been found to modulate weather and climate in East Asia (Li et al. 2010; Li and Ma 2011). Therefore, it is of great interest to examine whether the PMM modulates the occurrence of TCs in the WNP.

The objectives of this study are thus 1) to assess whether and to what extent the PMM modulates TC activity in the WNP and 2) to dissect the mechanisms underpinning the modulation based on both observations and model simulation. This study is expected to enhance the understanding of TC activity in the WNP and to provide valuable insights for seasonal forecasting of the occurrence of TCs over that region. Moreover, since the PMM is linked to extratropical climate systems such as the NPO (Rogers 1981; Linkin and Nigam 2008) and North Pacific Gyre Oscillation (NPGO) (Di Lorenzo et al. 2010), which is the second principal mode of SST anomalies in the North Pacific, this study can play a role in bridging the association of extratropical and tropical interactions (Vimont et al. 2001).

The remainder of this paper is organized as follows. Section 2 presents the data and methodology, while section 3 discusses the results based on observations and simulations. Section 4 includes the discussion and summarizes the main conclusions.

2. Data and methodology

a. Data

The TC data are obtained from International Best Track Archive for Climate Stewardship (IBTrACS; Knapp et al. 2010). The study period is 1961–2013 because TCs after the 1960s are more reliable (Chan 2008b). The key meteorological variables such as zonal and meridional wind fields, geopotential height, vorticity, and relative humidity are from the Japan Meteorology Agency (JMA) 55-year Reanalysis Project (JRA-55). To substantiate and reinforce the results, the National Centers for Environmental Prediction (NCEP)–National Center for Atmospheric Research (NCAR) reanalysis data (Kalnay et al. 1996) and the Modern-Era Retrospective Analysis for Research and Applications (MERRA) are also employed. The JRA-55 is available since 1958 on a global basis with a spatial resolution of 1.25° × 1.25°. It is based on a new data assimilation system that reduces many of the problems reported in the first JMA reanalysis (Ebita et al. 2011; Kobayashi et al. 2015). MERRA is produced by the National Aeronautics and Space Administration (NASA) for the satellite era, using a major new version of the Goddard Earth Observing System Model, version 5 (GEOS-5), data assimilation system (DAS) (Rienecker et al. 2011). MERRA data are only available from 1979. The zonal vertical wind shear ($|du/dz|$ or $|u_z|$) is defined as the magnitude of the differences in zonal wind between the 200- and 850-hPa levels. The years used in the above three reanalysis data are consistent with the TC data. Monthly estimates of SST are taken from the Met Office Hadley Centre Sea Surface Temperature dataset (HadSST3.1.1.0) (Kennedy et al. 2011).

b. Model

This study employs a newly developed high-resolution coupled climate model for experiments, the Geophysical Fluid Dynamics Laboratory (GFDL) Forecast-Oriented Low Ocean Resolution version of CM2.5 known as FLOR (e.g., Vecchi et al. 2014; Jia et al. 2015; Yang et al. 2015). The aim in the development of FLOR was to represent regional scales and extreme weather and climate events (e.g., TCs) while keeping computational costs relatively low. For these reasons, this model is characterized by high-resolution land and atmosphere components but a relatively low-resolution ocean component (Vecchi et al. 2014). The atmosphere and land are the same as those of the GFDL Climate Model, version 2.5 (CM2.5; Delworth et al. 2012), with a spatial resolution of 50 km × 50 km. The ocean and sea ice components of FLOR are similar to those in the CM2.1 (Delworth et al. 2006) with a spatial resolution of 1° × 1° except that there is refinement of the grid in the deep tropics (from 10°S to 10°N) to approximately ⅓° in meridional direction. The relatively low spatial resolution of the ocean and sea ice components in FLOR enables large ensembles and better efficiency for seasonal forecasting. This study utilizes the flux-adjusted version of FLOR (FLOR-FA) for sensitivity experiments in which climatological adjustments are applied to the model's momentum, enthalpy, and

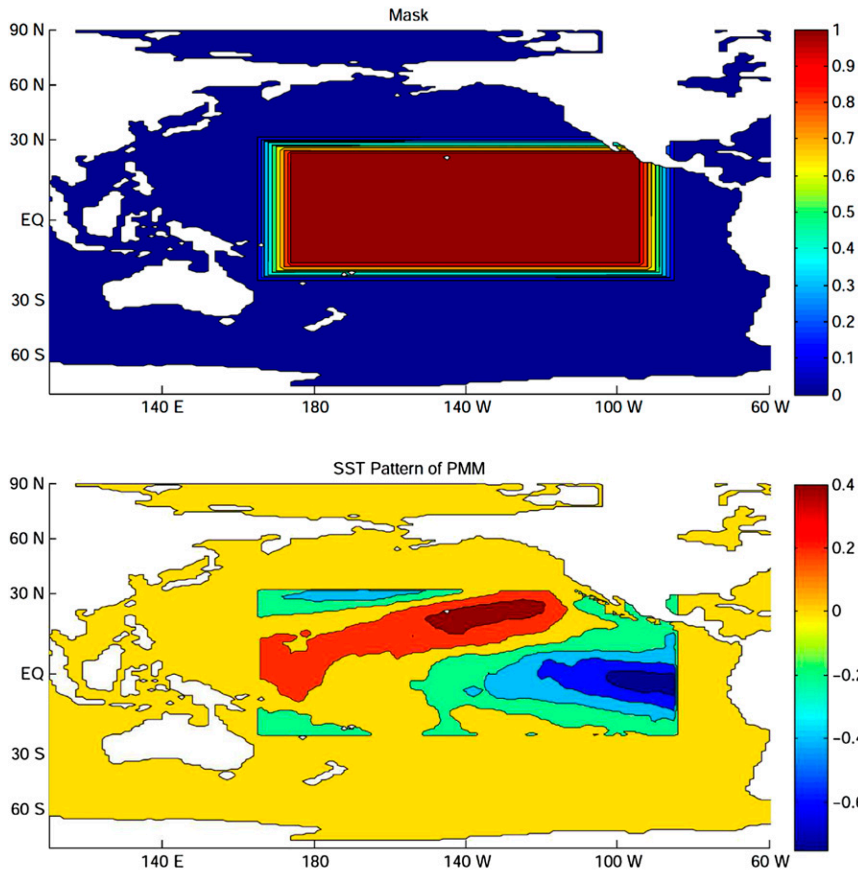

FIG. 2. (top) The restoring coefficient in the PMM region and (bottom) the SST anomalies (°C) during the positive PMM phase added to the seasonal cycle in the experiment.

freshwater flux from the atmosphere to the ocean to give the model's SST and surface wind stress a closer climatology to the observations over 1979–2012 (Vecchi et al. 2014). For more details about the FLOR model, please refer to Vecchi et al. (2014) and Jia et al. (2015), and references therein.

c. Control simulation

A 2500-yr-long control simulation was performed with the FLOR-FA by prescribing radiative forcing and land use representative of 1860. These experiments are referred to as pre-industrial experiments with FLOR-FA. The control experiments are run for a total of 2500 yr, but here we focus on the first 1000 yr for the analysis of PMM and TCs for the sake of computing efficiency. The PMM–TC relationship is also analyzed in another 500-yr control simulation, in which the prescribed radiative forcing and land use are representative of the conditions in 1990. Because the PMM–TC association based on FLOR-FA 1990 is consistent with that on FLOR-FA 1860, this study only shows results based on FLOR-FA 1860.

d. Sensitivity experiments

To isolate the role of the PMM, a set of perturbation experiments was performed with FLOR-FA using 1860 radiative forcing. In the first experiment, SST is restored to a repeating annual cycle in the PMM region (i.e., the masking region) and the model is fully coupled outside of the masking region with a 5-day restoring time scale, which is taken as the control run (CTRL) (Fig. 2). The second experiment is set up by prescribing the sum of the annual cycle of SST and the temporally constant SST anomalies associated with positive PMM patterns (denoted as PPMM) in the PMM region, with the model fully coupled outside of this region (Fig. 2). After an initial 100-yr spinup, both experiments are integrated for 100 yr. The restoring coefficient of the restoring SST is shown in Fig. 2, with the coefficient varying from 1 to 0 when moving from the center to the boundary of the masking region. By subtracting the CTRL experiment from the PPMM experiment, one can assess the net influence of the positive PMM phase on the climate system.

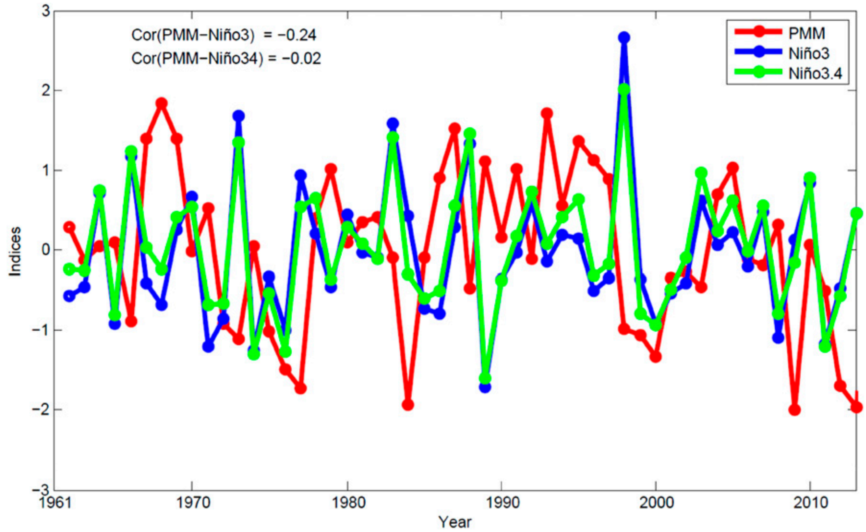

FIG. 3. The time series of the PMM (red), Niño-3 (blue), and Niño-3.4 (green) indices. Cor(PMM–Niño-3) represents the correlation coefficient between PMM and Niño-3 while Cor(PMM–Niño34) is defined likewise.

e. Tracking algorithm

TCs in FLOR are tracked from the 6-hourly model output by using the tracker developed by L. Harris et al. (unpublished manuscript) as implemented in Murakami et al. (2015). The temperature anomalies averaged vertically over 300 and 500 hPa (t_a) and sea level pressure (SLP) are key factors of this tracker. The tracking procedure is as follows.

1) Local minima of the smoothed SLP field are found. The location of the center is properly adjusted by fitting a biquadratic interpolation to the SLP and locating the center at the minimum.
2) Closed contours are constructed around every single SLP minimum with an interval of 2 hPa between the contours. The Nth contour is marked as the contiguous region surrounding a low central pressure P with pressures lower than $N\,dp + P$, as detected by a "flood fill" algorithm. This method works by starting at a seed point and adding neighboring grids to it that share the same desired properties. The boundary of the region iteratively grows outward until it reaches grids that no longer share the desired properties (Khudeev 2005). It is noted that the contours are not required to be circular and a maximum radius of 3000 km is searched from each candidate low center.
3) If the above closed contours are found, the low is counted as a TC center at that time. In this way, the tracker attempts to find all closed contours within a certain distance of the low and without entering contours belonging to another low. The maximum 10-m wind inside the set of closed contours is taken as the maximum wind speed at that time for the storm.
4) Warm cores are detected via similar processes: closed 1-K contours for FLOR are found surrounding a maximum of t_a within the previously identified SLP minima, no more than 1° from the center of minimum SLP. This contour must have a radius less than 3° in distance. If such a core is not found, it should not be defined as a warm-core low center and the center is rejected.
5) TC centers are combined into a track by taking a low center at time $T - dt$, extrapolating its motion forward dt, and then seeking for storms within 750 km. It is noted that the lower local minimum SLP has higher priority to be joined to the current minimum to form the TC track.
6) The following criteria are required to pick up the final TCs:
   (i) a lifespan of at least 72 h,
   (ii) at least 48 cumulative (not necessarily consecutive) hours with a warm core, and
   (iii) at least 36 consecutive hours of a warm core with winds greater than 17.5 m s^{-1}.

TC genesis is confined equatorward of 40°N. TC density is obtaining by binning the 6-hourly TC tracks in the WNP in 5° × 5° grid boxes.

f. PMM index

The PMM index (Fig. 3) is calculated following the method described in Chiang and Vimont (2004). In calculating it, the seasonal cycle and the linear trend are first removed by applying a 3-month running mean to the data, and then subtracting the linear fit to the CTI (Deser and Wallace 1987) from every single spatial point to remove correlations with El Niño (Chiang and Vimont 2004). The CTI is defined as the average SST anomaly over 6°N–6°S, 180°–90°W minus the global mean SST (Deser and Wallace 1987).

The correlation coefficients between the time series of PMM and Niño-3 (5°S–5°N, 150°–90°W) is −0.24 while that between PMM and Niño-3.4 is −0.02 (Fig. 3). Although the correlation between PMM and Niño-3 is relatively weak, we also analyze the PMM–TC association in the WNP during the neutral ENSO years to assess to what extent such association is influenced by ENSO. The El Niño (La Niña) years are defined as those with Niño-3 values during July–October larger than 1 (smaller than −1) standard deviation. This definition is applied to both observations and long-term control run with FLOR-FA. The PMM pattern during the period 1961–2013 strongly resembles that during the neutral ENSO years (shown in Figs. 1a and 1b), suggesting that the PMM pattern is hardly influenced by the ENSO events.

The peak season for TCs is defined as July–October. The results are consistent if we slightly change the definition of the TC peak season from June to November or from July to November (not shown).

3. Results

The analysis results of the PMM–TC association are derived from observations, a 1000-yr FLOR-FA control experiment, and sensitivity experiments based on FLOR-FA.

a. Observations

The regressions of SST and 10-m wind fields onto the PMM index in observations are shown in Fig. 1. There is a characteristic pattern to the PMM in the central and eastern Pacific, with warming in the northwestern part (subtropical) and cooling in the southeastern part (tropical) (Fig. 1). The warming in the central Pacific is in the vicinity of the WNP and may affect TC activity there. The PMM pattern during 1961–2013 and that during neutral ENSO years are consistent (Figs. 1a and 1b), suggesting that ENSO marginally influences the PMM pattern.

The regressions of TC track density onto the PMM index for 1961–2013 are largely positive in the WNP in the observations, indicating that TC activity is enhanced (suppressed) in the WNP in the positive (negative) PMM phase (Fig. 1c). In addition, we calculate the correlation between the time series of the PMM index and the TC frequency in the WNP for the period of 1961–2013. For each year, the PMM index is calculated by averaging the monthly PMM index over the peak TC season (July–October). The correlation coefficient between the two is 0.46, significant at the 0.01 level (Fig. 4a). Previous studies have argued that the occurrence of the PMM is independent of ENSO (L. Zhang et al. 2009; Larson and Kirtman 2014), and the linear ENSO effect has been removed when calculating the PMM index. To further exclude the linear influence of ENSO on the PMM–TC association, we also analyze the PMM–TC association during neutral ENSO years only and the partial correlation by controlling the Niño-3 index. The linear fitting line during neutral ENSO years strongly resembles that for the period 1961–2013 (Fig. 4a). The partial correlation between WNP TC frequency and PMM by controlling the Niño-3 index is still significant at the 0.01 level of significance (Fig. 5).

To analyze the observed relationship between WNP TC genesis and PMM, the WNP is divided into five subregions following the definition of subregions in the WNP in Wang et al. (2013): the South China Sea (SCS) and the northwestern part (NW), northeastern part (NE), southwestern part (SW), and southeastern part (SE) (Fig. 5). The SE has a relatively high density of TC genesis (Fig. 5). The PMM index has a significant positive Spearman correlation with TC frequency in the SE, NE, and NW (Fig. 5). The partial correlation by controlling Niño-3 is consistent with the Spearman correlation except for the NW of the WNP in that the Spearman correlation is significant while the partial correlation is insignificant (Fig. 5).

To further assess which large-scale atmospheric conditions may be acting to modulate the TC occurrence, a suite of variables associated with TC genesis (Chan 2000; Wang and Chan 2002) based on JRA-55 is regressed onto the PMM index (Fig. 6). Chan and Liu (2004) found that the increase in local SST has no significant influence on TC activity in the WNP. Indeed, the modulation of local large-scale circulation by remote SST anomalies (e.g., ENSO) largely leads to changes in TC activity there (Chan, 2000; Wang and Chan, 2002; Chan and Liu, 2004; Camargo and Sobel, 2005). Therefore, instead of analyzing local SST, we analyze 600-hPa relative humidity, 850-hPa relative vorticity, and zonal vertical wind shear (ZVWS) for TC genesis. These environmental variables are the same as those responsible for the modulation of ENSO on WNP TC genesis used in Camargo et al. (2007). In general, the regressions of the PMM index on the JRA-55, NCEP–NCAR, and MERRA reanalysis data are consistent. Thus, we only show the results from JRA-55 reanalysis

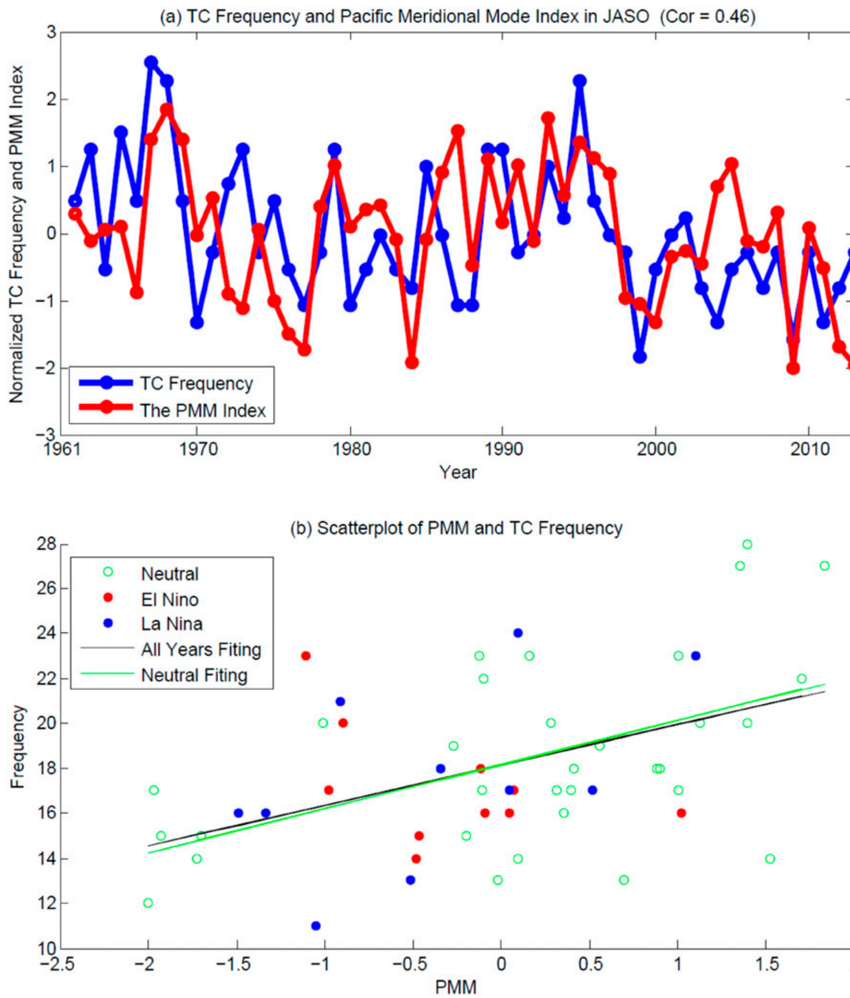

FIG. 4. (a) The standardized time series of the annual PMM index and WNP TC frequency for the period 1961–2013 and (b) scatterplot of PMM vs WNP TC frequency in El Niño (red dots), La Niña (blue dots), and neutral ENSO years (green circles); the fitted lines indicate all years of 1961–2013 (black line) and only neutral ENSO years (green line). The annual PMM index and WNP TC frequency are calculated by averaging over July–October.

data. The regression of ZVWS is characterized by strong negative anomalies in a large portion of the WNP (0°–20°N, 120°E–180), which would act to enhance TC genesis (Fig. 6). Further analysis indicates that the changes in ZVWS arise from anomalous westerlies (easterlies) at the 850-hPa (200 hPa) level although the anomalous westerlies at 850 hPa is mainly located in the western part of the WNP (Fig. 6). Such anomalous winds in the lower and upper levels can weaken the prevalent westerlies in the upper level (200 hPa) and the prevalent easterlies (850 hPa) in the lower level over the WNP. The spatial patterns dramatically resemble a classic Gill (1980) response to off-equatorial heating (Fig. 6). The mechanisms underlying how the vertical wind shear is modulated by the large-scale circulation will be discussed in detail in section 3c. The AMM pattern (the Atlantic counterpart of PMM) also has a significant positive correlation with hurricane frequency in the North Atlantic because of increased subtropical SST, convergence, and low sea level pressure and decreased vertical wind shear (Vimont and Kossin 2007; Smirnov and Vimont 2011).

b. *Results from the long-term control run*

The 1000-yr control simulation of FLOR-FA with 1860 radiative forcing is analyzed to further understand the PMM–TC association. The main purpose is to test whether such a PMM–TC association also holds for the long-term control simulation of FLOR-FA, which would provide a dynamical framework in which to

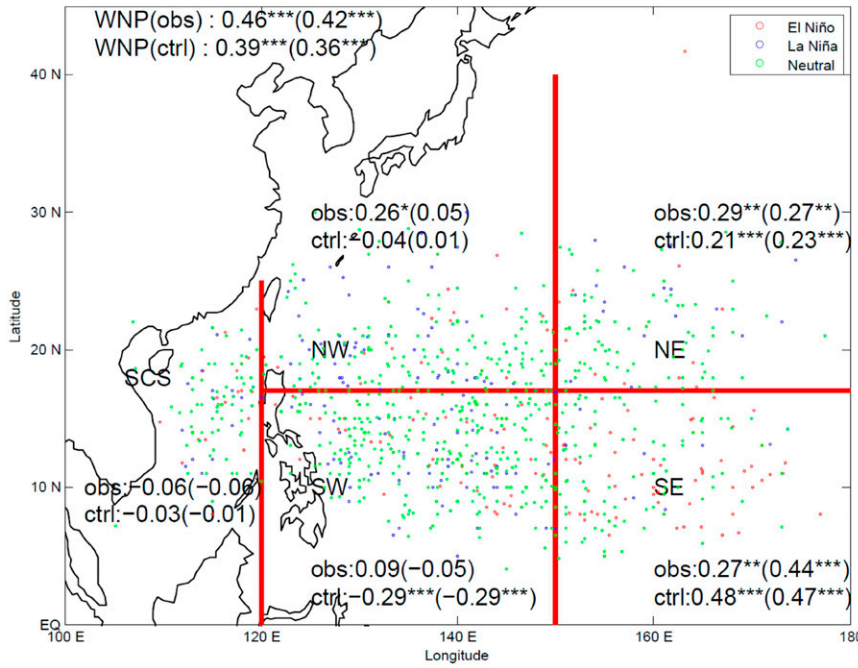

FIG. 5. The five subregions of TC genesis in the WNP. Blue dots represent TC genesis locations in the period of 1961–2013. Here obs denotes the correlation between PMM and TC frequency in observations whereas ctrl denotes that in control run. The numbers following obs or ctrl denote correlation coefficients in each subregion. WNP(obs) represents the correlation coefficient between PMM and TC frequency in the WNP in the observations while WNP(ctrl) denotes that in control run (1000 yr). The numbers in the parentheses represent partial correlation. One, two, and three asterisks represent a significance level of 0.1, 0.05, and 0.01, respectively. The red, blue, and green dots denote the TC genesis locations during El Niño, La Niña, and neutral ENSO years, respectively.

understand the causes of this connection. The PMM index in the control experiment is also calculated based on the method proposed in Chiang and Vimont (2004). The PMM in the FLOR-FA control simulation (Fig. 7a) captures the fundamental features of the observed PMM (Fig. 1a), indicating that the FLOR-FA model is capable of simulating the basic structure of the PMM in a fully coupled numerical climate system. The PMM pattern in FLOR-FA control simulation during neutral ENSO years (Fig. 7b) is consistent with those during the 1000 years (Fig. 7a), indicating a weak influence of ENSO on the PMM pattern in the long-term control run. Despite the resemblance in the PMM pattern between observations and model simulation, the control experiment of FLOR-FA produces a weaker cooling and 10-m wind fields in the southeastern part of PMM, and stronger cooling northwest of the positive anomalies compared to the observations. In addition, the squared covariance fraction of the PMM in the observations is 53% (Chiang and Vimont 2004) whereas it is 30% in the control experiment, suggesting a weaker role of PMM in the control experiment.

The regression of TC track density on the PMM index is generally positive in the WNP in the control experiment (1000 yr; Fig. 7c), consistent with the observations (Fig. 1c). However, the positive regressions are largely confined in the southeastern WNP (Fig. 7b). The correlation coefficient between the simulated PMM and WNP TC frequency is 0.37 for the 1000-yr simulation, significant at 0.01 level of significance (Fig. 8a). The fitting lines during the 1000 years and the neutral ENSO years of the control run have similar slope, suggesting that ENSO exerts a weak modulation on the PMM–WNP TC relationship (Fig. 8a). Figure 8b shows the histogram of the correlation coefficients in moving 50-yr chunks and all are positive. The correlation coefficient from the observations is within the model spread. This suggests consistency between the observed and modeled TC–PMM association, as the observed correlation falls well within the spread of the model correlations. The partial correlation by controlling Niño-3 and that during only neutral ENSO years of the 1000-yr control run are similar to each other, significant at the 0.01 level (Fig. 8b).

The model shows negative anomalies in ZVWS in the southeastern part (0°–20°N, 150°E–180°) of the

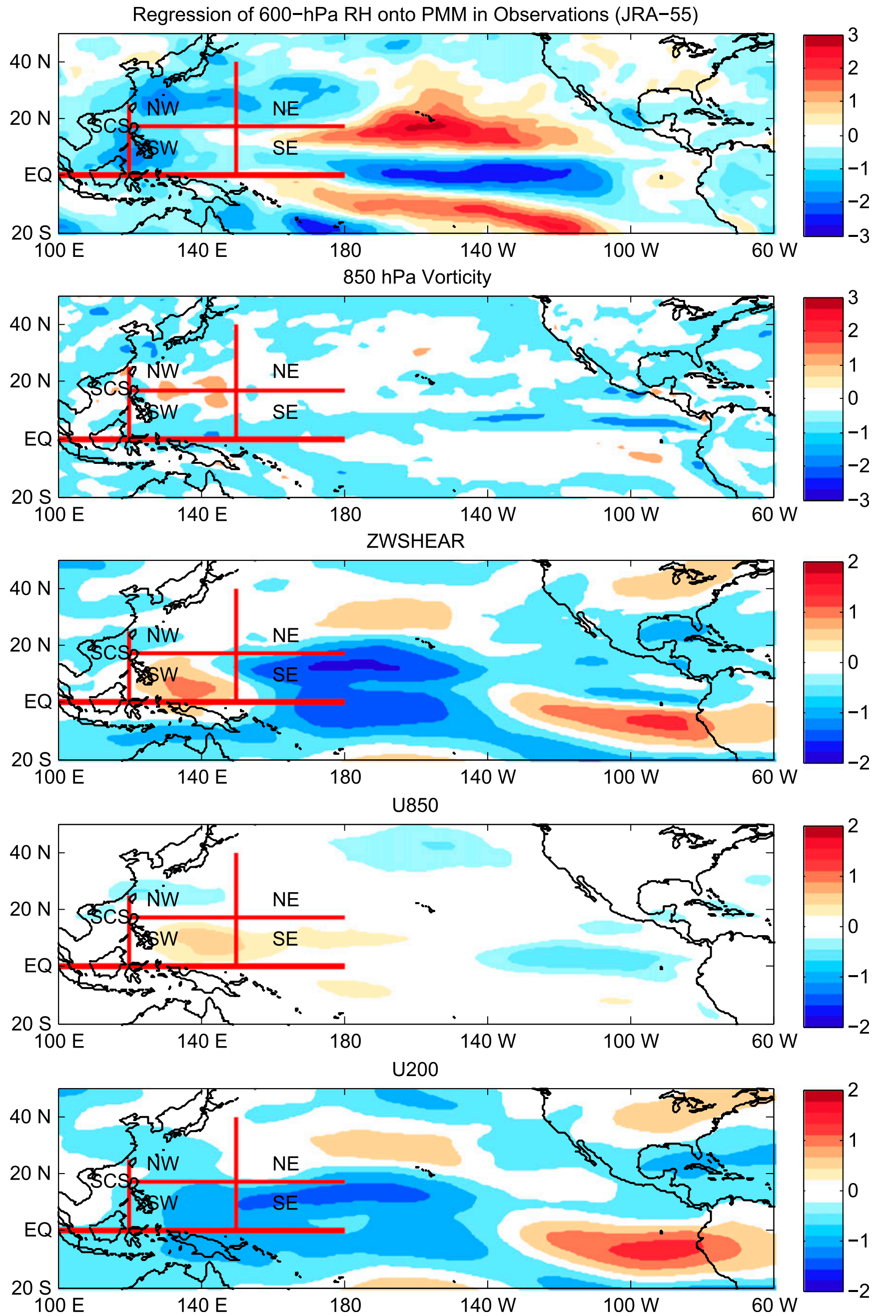

FIG. 6. The regressions of 600-hPa relative humidity (%), 850-hPa relative vorticity ($10^{-6}\,s^{-1}$), zonal vertical wind shear ($m\,s^{-1}$), 850-hPa wind ($m\,s^{-1}$), and 200-hPa wind ($m\,s^{-1}$) onto the PMM index based on JRA-55. The thick red lines are used to divide the five subregions in the WNP.

WNP (Fig. 9), similar to those based on observations (Fig. 6). There are positive anomalies of ZVWS westward of 150°E in the control experiment, suggesting unfavorable condition for TC genesis there. This is responsible for the different spatial patterns for TC genesis between the observations and control simulation (Fig. 5). The observations show that TC genesis is promoted in almost all the subregions in the observations (Fig. 5). In contrast, the control simulation shows that TC genesis is enhanced in the southeastern part while suppressed in the southwestern subregion of the WNP (Fig. 5). It is noted that we have also analyzed the 500-yr FLOR-FA control with 1990 radiative forcing and the results derived from both control runs are consistent in terms of the PMM pattern and TC–PMM association.

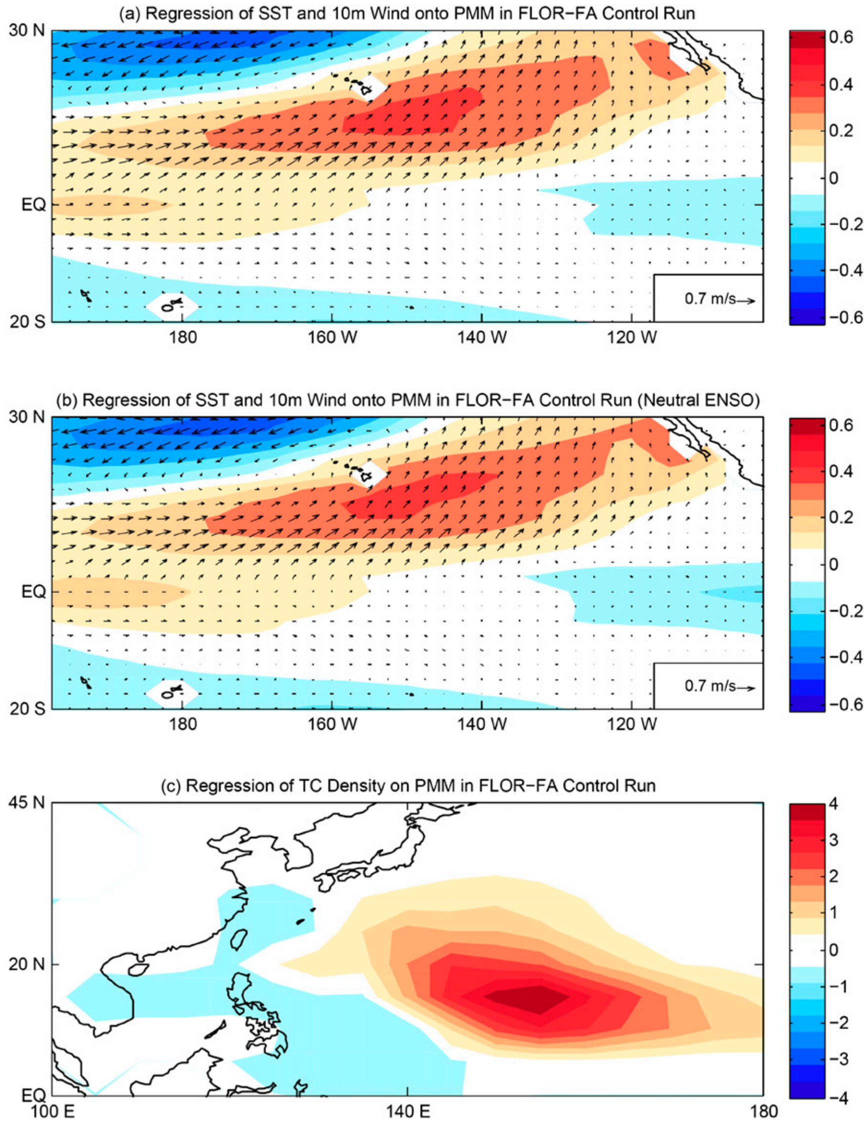

FIG. 7. Regression of SST anomalies (°C) and 10-m wind fields ($m\,s^{-1}$) during (a) all 1000 yr and (b) neutral ENSO years, and (c) regression of TC density onto the standardized PMM index in a 1000-yr control simulation of the FLOR-FA.

In summary, the 1000-yr control experiment produces quantitatively consistent results with observation, with positive phases of the PMM conducive to WNP TC genesis, and anomalous reductions of ZVWS during the positive PMM phases. However, TC genesis exhibits different regional relationships between observations and the control experiment, which may be explained by different anomalous ZVWS patterns in the model and observations. To further investigate the mechanisms underpinning how PMM modulates TC genesis in the WNP, a set of sensitivity experiments have been performed using FLOR-FA and will be discussed in next subsection.

c. *Results from sensitivity experiments*

To isolate the role of the PMM, a set of perturbation experiments were performed with FLOR-FA using 1860 radiative forcing. The description of the perturbation experiments is provided in section 2d. One can assess the net influence of the positive PMM phase on the climate system by subtracting the CTRL experiment from the PPMM experiment.

The mean WNP TC frequency during the peak TC season [July–October (JASO)] in the 100-yr PPMM experiment (19.4) is significantly higher than the control experiment (17.5) at the 0.01 significance level (Table 1).

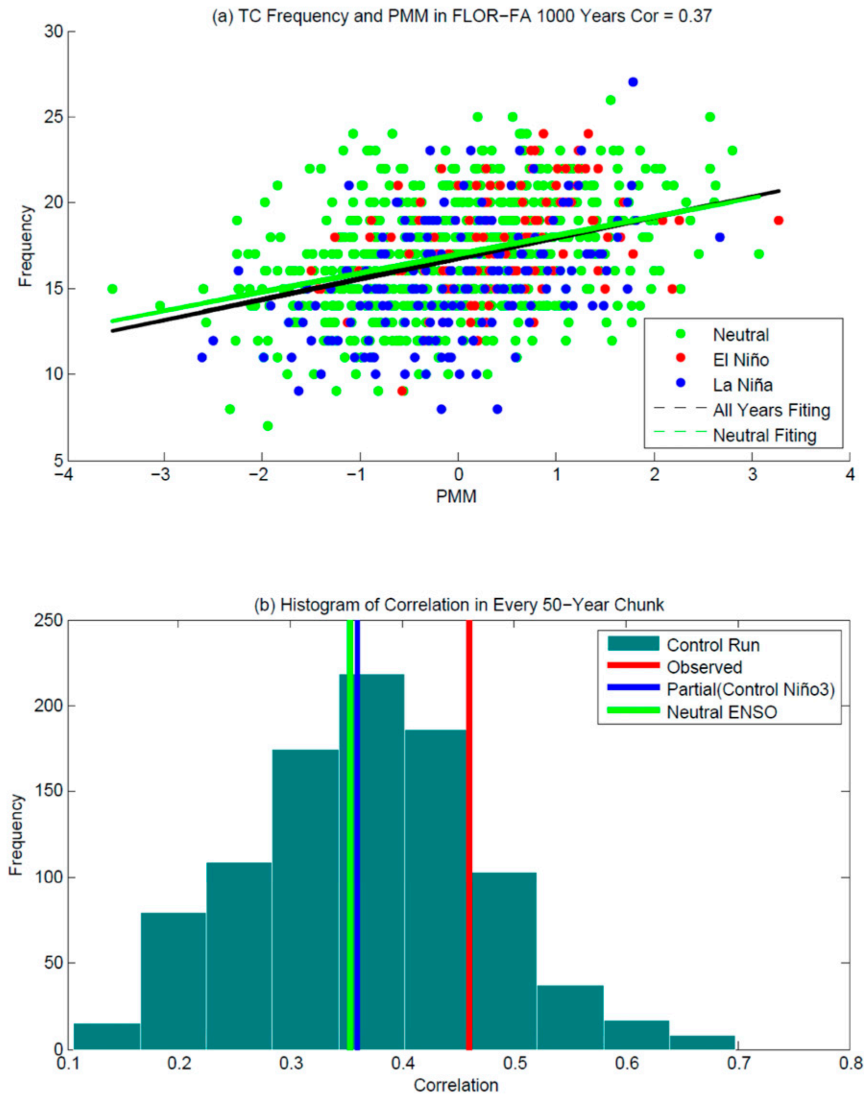

FIG. 8. (a) The scatterplot of PMM vs WNP TC frequency (blue dots) and fitted line (black), and (b) the histogram of correlation between WNP TC frequency and PMM for every 50 yr in the control experiment of FLOR-FA. The correlation between WNP TC frequency and PMM based on observations is shown in the thin red bar. The thin blue bar and green bar denote the partial correlation between WNP TC frequency and PMM by controlling Niño-3 and that during neutral ENSO years only.

The difference in WNP TC frequency between the PPMM experiment (26.7) and CTRL (24.7) is also significant for June–November (JJASON) (Table 1). To better represent the differences between the two experiments, TC density is computed by binning TC centers in $5^\circ \times 5^\circ$ grid boxes in the WNP. Positive anomalies of TC density are observed in the eastern part of the WNP (Fig. 10). However, the positive anomalies have higher magnitude than the negative ones. These positive anomalies arise from an enhanced TC genesis in the PPMM experiment (Fig. 11). The occurrence of TC genesis in the PPMM experiment is higher than that in the control run in the eastern part of the WNP (Fig. 11). These experiments corroborate that the positive PMM phases promote TC genesis in the WNP, especially in the eastern portion of the WNP. A number of studies have proposed mechanisms on how remote SST patterns affect TC genesis in the WNP, including the Matsuno–Gill pattern (Matsuno 1966; Gill 1980), Pacific–East Asia teleconnections (Wang et al. 2000; Wang and Chan 2002), the Philippine anticyclone induced by Indian Ocean warming (Xie et al. 2009; Ha et al. 2015), and SST

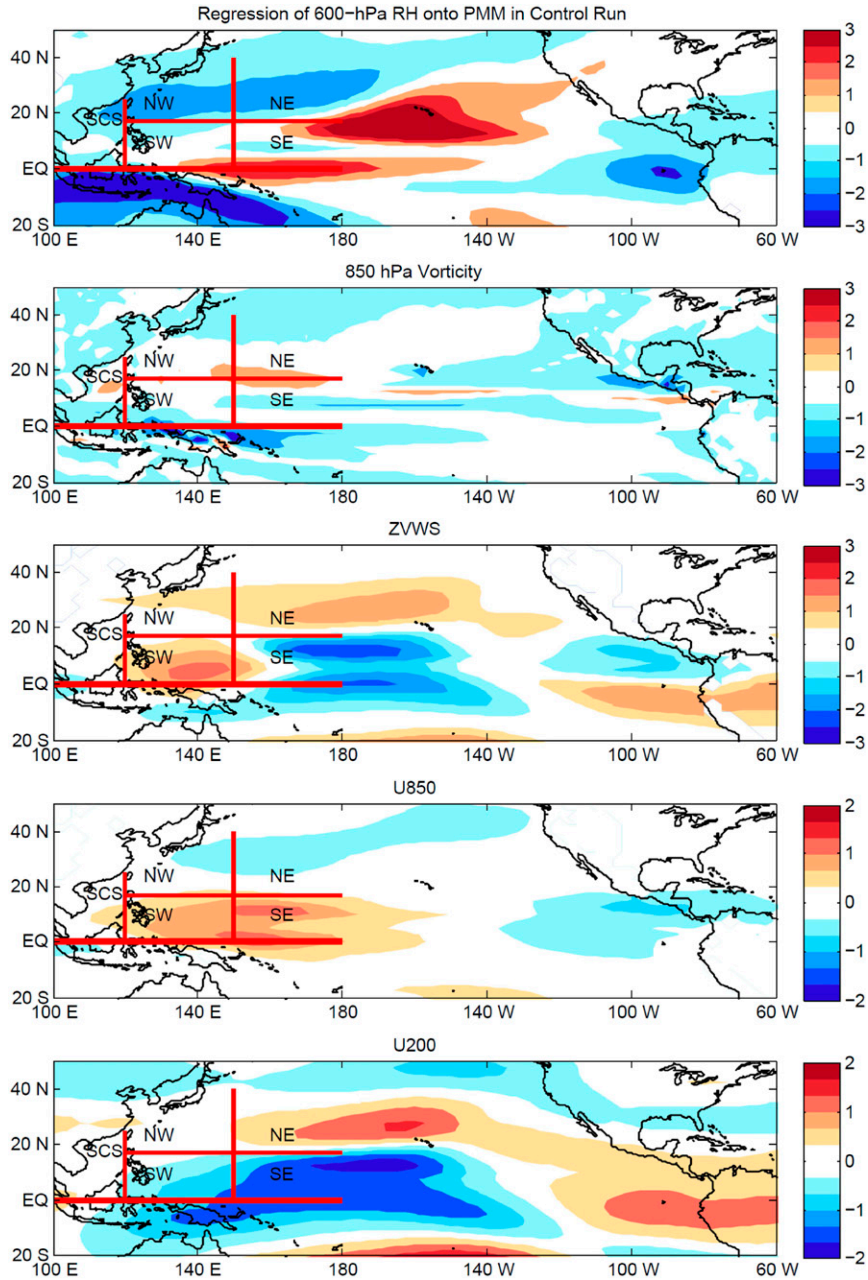

FIG. 9. The regressions of 600-hPa relative humidity (%), 850-hPa vorticity ($10^{-6}\,s^{-1}$), zonal vertical wind shear ($m\,s^{-1}$), 850-hPa wind ($m\,s^{-1}$), and 200-hPa wind ($m\,s^{-1}$) onto the PMM index in the control experiment of FLOR-FA. The thick red lines are used to divide the five subregions in the WNP.

gradients (Zhan et al. 2013; Li and Zhou 2014). These studies have emphasized the importance of the Philippine anticyclone and monsoon trough in modulating TC genesis and how SST anomalies modulate the large-scale circulation in remote areas.

To explain why TC genesis in the PPMM experiment is higher in the eastern part of the WNP, the large-scale atmospheric factors related to TC genesis are analyzed. The differences between the PPMM and control run resemble the regression of those variables onto the PMM index in both control experiment and observations (Fig. 12). This suggests that the SST pattern in the positive PMM phase and within that particular box drives the modeled and observed TC genesis in the

TABLE 1. TC frequencies in JASO and JJASON for PPMM and CTRL experiment. Boldface numbers represent the differences that are statistically significant, with an asterisk representing results significant at the 0.01 level based on Student's t test.

Frequency	JJASON	JASO
PPMM	26.7	19.4
CTRL	24.7	17.5
PPMM − CTRL	**2.0***	**1.9***

WNP, especially in its eastern part. Specifically, negative anomalies of ZVWS are induced by the PPMM, arising from westerly anomalies at the 850-hPa level and easterly anomalies at 200 hPa (Fig. 12). These changes can be described as a change in the Walker circulation. The question is then related to the mechanisms that lead to the changes in the Walker circulation. It is known that the positive PMM pattern features a warming in the northwestern part and a cooling in the southeastern part in the tropical eastern Pacific (Figs. 1, 7, and 13). A cyclonic 850-hPa flow is forced by the anomalous warming in the tropical central Pacific through the Matsuno–Gill response (Matsuno 1966; Gill 1980). The responses to anomalous positive PMM warming are quite similar to the Matsuno–Gill pattern under asymmetric heating (Gill 1980), showing that a cyclonic pattern is located northwestward of the heating (Fig. 13). In addition, the diabatic heating center can also be identified by negative outgoing longwave radiation (OLR) anomalies (Fig. 13). The anomalous cyclonic flow pattern in the WNP is more likely to cause a weaker Philippine

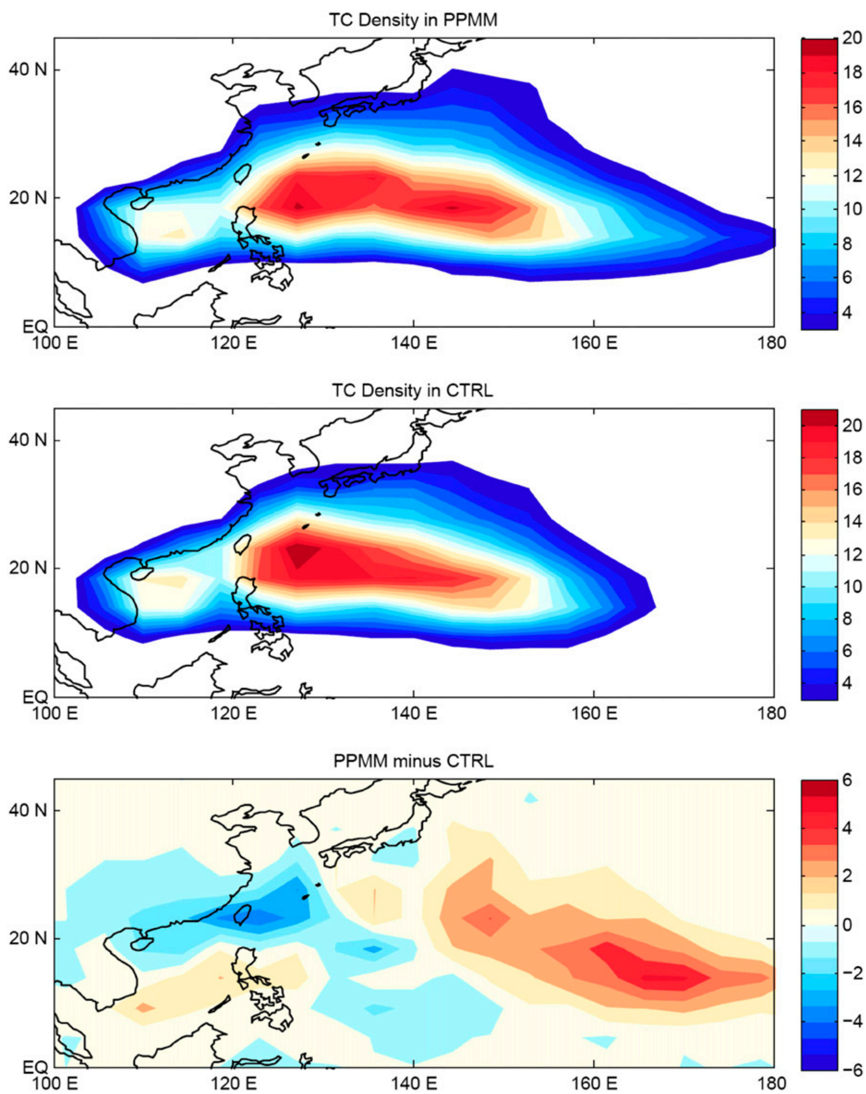

FIG. 10. TC track density in the (top) PPMM experiment and (middle) CTRL experiment, and (bottom) the difference PPMM − CTRL.

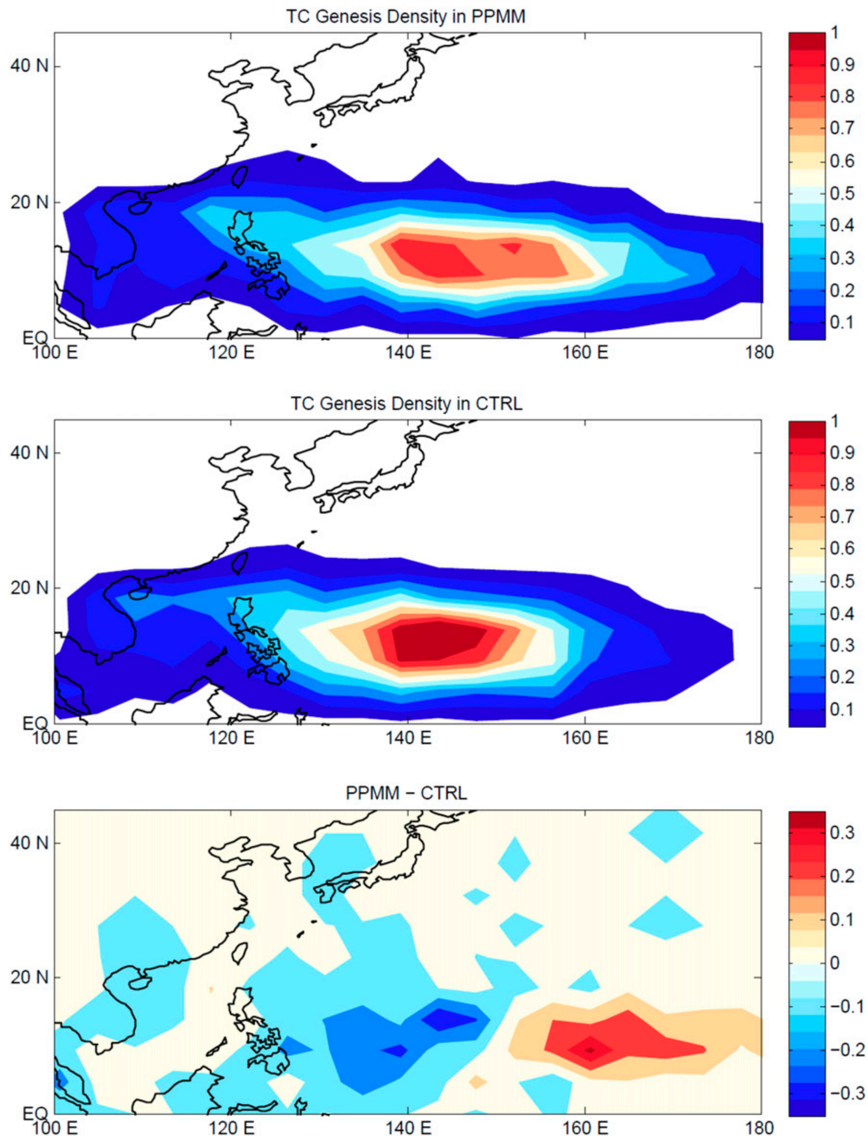

FIG. 11. As in Fig. 10, but for TC genesis.

anticyclone, a weaker subtropical high, and an elongated monsoon trough, which are favorable conditions for TC genesis in the WNP (Wang et al. 2000; Wang and Chan 2002). Intensified low-level westerly and easterly flows move toward the PPMM heating center from east and west, respectively (Fig. 13). The enhanced TC genesis in the WNP can be attributed to weaker ZVWS, which arises from the responses of the atmosphere to the anomalous warming that is part of the positive PMM pattern via the Matsuno–Gill mechanisms.

4. Discussion and conclusions

The Pacific meridional mode (PMM) has been the subject of heightened interest by the scientific community because of its role in bridging across the extratropical and tropical climate systems. It is thus of high scientific relevance whether the PMM is linked to TCs in the WNP given that previous studies claimed that its counterpart AMM is intimately associated with hurricane activity in the North Atlantic (Vimont and Kossin 2007; Smirnov and Vimont 2011; Patricola et al. 2014).

This study has analyzed the observed and modeled association between the PMM and TC activity in the WNP. Our results show that the positive PMM phase promotes the occurrence of TCs in the WNP. There is a general consistency in the diagnostic TC–PMM relationship in observations and in a long-term control experiment (1000 yr) of FLOR-FA. Sensitivity experiments using the model show causality in the PMM–TC

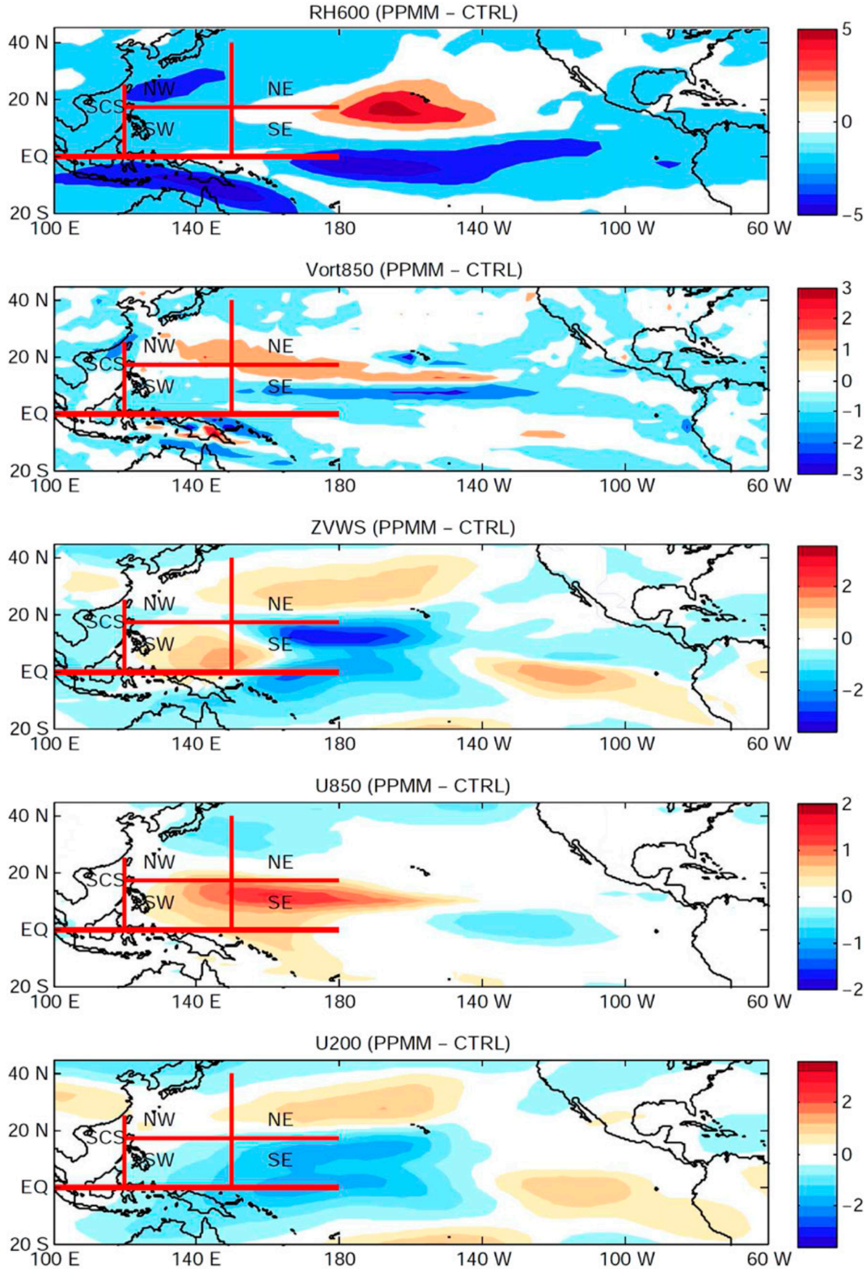

FIG. 12. The differences in 600-hPa relative humidity (%), 850-hPa relative vorticity ($10^{-6}\,s^{-1}$), ZVWS (200–850-hPa, $m\,s^{-1}$), 850-hPa wind ($m\,s^{-1}$), and 200-hPa wind ($m\,s^{-1}$) between PPMM and control experiments. The thick red lines are used to divide the five subregions in the WNP.

relation. The modulation of the TC genesis by the PMM originates mainly from the abnormal ZVWS in the WNP, especially in its southeastern portion as shown in the control and sensitivity experiments. The anomalous ZVWS is attributable to the responses to the atmosphere to the anomalous warming in the positive PMM pattern through Matsuno–Gill mechanisms. Such results are supported by the cyclonic flow in the Philippine Sea and relevant flow patterns over the Pacific Ocean in the sensitivity experiments.

The PMM is linked to the climate modes in the North Pacific such as NPO and NPGO (Chiang and Vimont, 2004). For example, the NPO, which is the atmospheric component of NPGO, tends to force the PMM (Chiang and Vimont 2004). Therefore, the PMM bridges the extratropical and tropical climate systems. As shown in

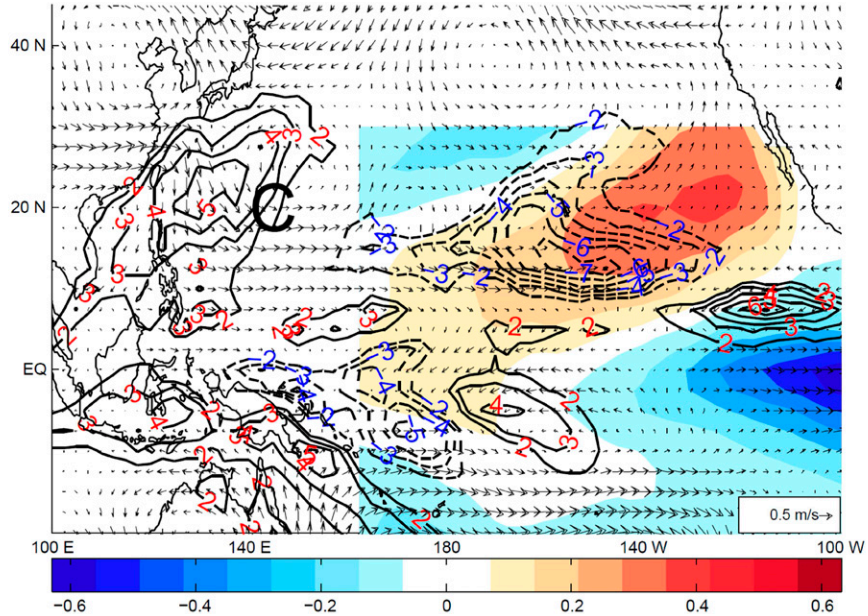

FIG. 13. The differences in 850-hPa wind fields (vector, $m\,s^{-1}$) and OLR (contour, $W\,m^{-2}$) between PPMM and CTRL experiments with FLOR-FA, and the SST pattern of the positive PMM pattern (shading, °C). The capital letter C denotes cyclonic flow.

Zhang et al. (2013), the NPGO/NPO modulates the occurrence of TCs in the WNP and it plays an even stronger role than ENSO and PDO based on the observations. In addition, Chen et al. (2015) reported that the spring NPO can modulate TC activity in the WNP in the following peak TC season. However, detailed mechanisms are yet to be unraveled. This study may provide some hints to explain the impacts of the NPGO or NPO on TCs in the WNP.

It is known that the PMM pattern is obtained by removing the effect of ENSO via linear removal of the cold tongue index (Deser and Wallace 1990). TCs in the WNP are affected by various climate modes such as ENSO, the Indian Ocean basin mode (IOBM), NPGO, PDO, and the SST in the North Atlantic Ocean. This study has also found that the PMM significantly modulates the occurrence of TCs in the WNP. Our ongoing study is examining the relative roles the climate modes play in influencing TC genesis in the WNP. Given the importance of the PMM in modulating the climate, the linkage between PMM and TC activity in other ocean basins will be analyzed in our future work. Moreover, the results of this study indicate that the predictability of the PMM is potentially of great value for the prediction of TC activity; future studies will examine the predictability of the PMM and TCs by leveraging seasonal forecasting experiments with FLOR-FA.

Although this study has found a significant relationship between PMM and WNP TC activity, it still has limitations. First, the removal of ENSO from PMM is not perfectly clean in this study and the PMM–TC linkage found may be influenced by this removal. Second, there exist uncertainties and biases (e.g., genesis regions and TC track density) in the model simulations. Third, the limited duration and biases of the observations plague to some extent the TC–climate analyses.

Acknowledgments. The authors are grateful to Dan Vimont and Suzana Camargo for their insightful comments and suggestions that improved this paper. This material is based in part upon work supported by the National Science Foundation under Grant AGS-1262099. The authors thank Xiaosong Yang and Andrew Wittenberg for their valuable comments on an earlier version of this paper. WZ benefitted from discussion with Lakshmi Krishnamurthy on this study. The authors thank Seth Underwood and Fanrong Zeng for their helpful assistance in experiments.

REFERENCES

Alexander, M. A., L. Matrosova, C. Penland, J. D. Scott, and P. Chang, 2008: Forecasting Pacific SSTs: Linear inverse model predictions of the PDO. *J. Climate*, **21**, 385–402, doi:10.1175/2007JCLI1849.1.

Camargo, S. J., and A. H. Sobel, 2005: Western North Pacific tropical cyclone intensity and ENSO. *J. Climate*, **18**, 2996–3006, doi:10.1175/JCLI3457.1.

——, K. A. Emanuel, and A. H. Sobel, 2007: Use of a genesis potential index to diagnose ENSO effects on tropical cyclone genesis. *J. Climate*, **20**, 4819–4834, doi:10.1175/JCLI4282.1.

Chan, J. C. L., 1985: Tropical cyclone activity in the northwest Pacific in relation to the El Niño–Southern Oscillation phenomenon. *Mon. Wea. Rev.*, **113**, 599–606, doi:10.1175/1520-0493(1985)113<0599:TCAITN>2.0.CO;2.

——, 2000: Tropical cyclone activity over the western North Pacific associated with El Niño and La Niña events. *J. Climate*, **13**, 2960–2972, doi:10.1175/1520-0442(2000)013<2960:TCAOTW>2.0.CO;2.

——, 2008a: A simple seasonal forecast update of tropical cyclone activity. *Wea. Forecasting*, **23**, 1016–1021, doi:10.1175/2008WAF2007061.1.

——, 2008b: Decadal variations of intense typhoon occurrence in the western North Pacific. *Proc. Roy. Soc. London*, **464A**, 249–272, doi:10.1098/rspa.2007.0183.

——, and K. S. Liu, 2004: Global warming and western North Pacific typhoon activity from an observational perspective. *J. Climate*, **17**, 4590–4602, doi:10.1175/3240.1.

Chang, P., L. Zhang, R. Saravanan, D. J. Vimont, J. C. H. Chiang, L. Ji, H. Seidel, and M. K. Tippett, 2007: Pacific meridional mode and El Niño–Southern Oscillation. *Geophys. Res. Lett.*, **34**, L16608, doi:10.1029/2007GL030302.

Chen, D., H. Wang, J. Liu, and G. Li, 2015: Why the spring North Pacific Oscillation is a predictor of typhoon activity over the western North Pacific. *Int. J. Climatol.*, **35**, 3353–3361, doi:10.1002/joc.4213.

Chiang, J. C. H., and D. J. Vimont, 2004: Analogous Pacific and Atlantic meridional modes of tropical atmosphere–ocean variability. *J. Climate*, **17**, 4143–4158, doi:10.1175/JCLI4953.1.

Delworth, T. L., and Coauthors, 2006: GFDL's CM2 global coupled climate models. Part I: Formulation and simulation characteristics. *J. Climate*, **19**, 643–674, doi:10.1175/JCLI3629.1.

——, and Coauthors, 2012: Simulated climate and climate change in the GFDL CM2.5 high-resolution coupled climate model. *J. Climate*, **25**, 2755–2781, doi:10.1175/JCLI-D-11-00316.1.

Deser, C., and J. M. Wallace, 1987: El Niño events and their relation to the Southern Oscillation: 1925–1986. *J. Geophys. Res.*, **92**, 14 189–14 196, doi:10.1029/JC092iC13p14189.

——, and ——, 1990: Large-scale atmospheric circulation features of warm and cold episodes in the tropical Pacific. *J. Climate*, **3**, 1254–1281, doi:10.1175/1520-0442(1990)003<1254:LSACFO>2.0.CO;2.

Di Lorenzo, E., K. Cobb, J. Furtado, N. Schneider, B. Anderson, A. Bracco, M. Alexander, and D. Vimont, 2010: Central Pacific El Niño and decadal climate change in the North Pacific Ocean. *Nat. Geosci.*, **3**, 762–765, doi:10.1038/ngeo984.

Du, Y., L. Yang, and S.-P. Xie, 2011: Tropical Indian Ocean influence on northwest Pacific tropical cyclones in summer following strong El Niño. *J. Climate*, **24**, 315–322, doi:10.1175/2010JCLI3890.1.

Ebita, A., and Coauthors, 2011: The Japanese 55-year Reanalysis "JRA-55": An interim report. *SOLA*, **7**, 149–152, doi:10.2151/sola.2011-038.

Gill, A. E., 1980: Some simple solutions for heat-induced tropical circulation. *Quart. J. Roy. Meteor. Soc.*, **106**, 447–462, doi:10.1002/qj.49710644905.

Girishkumar, M. S., V. P. Thanga Prakash, and M. Ravichandran, 2014: Influence of Pacific decadal oscillation on the relationship between ENSO and tropical cyclone activity in the Bay of Bengal during October–December. *Climate Dyn.*, **44**, 3469–3479, 10.1007/s00382-014-2282-6.

Gray, W. M., 1968: Global view of the origin of tropical disturbances and storms. *Mon. Wea. Rev.*, **96**, 669–700, doi:10.1175/1520-0493(1968)096<0669:GVOTOO>2.0.CO;2.

Ha, Y., Z. Zhong, X. Yang, and Y. Sun, 2015: Contribution of East Indian Ocean SSTA to western North Pacific tropical cyclone activity under El Niño/La Niña conditions. *Int. J. Climatol.*, **35**, 506–519, doi:10.1002/joc.3997.

Henderson-Sellers, A., and Coauthors, 1998: Tropical cyclones and global climate change: A post-IPCC assessment. *Bull. Amer. Meteor. Soc.*, **79**, 19–38, doi:10.1175/1520-0477(1998)079<0019:TCAGCC>2.0.CO;2.

Huo, L., P. Guo, S. N. Hameed, and D. Jin, 2015: The role of tropical Atlantic SST anomalies in modulating western North Pacific tropical cyclone genesis. *Geophys. Res. Lett.*, **42**, 2378–2384, doi:10.1002/2015GL063184.

Jia, L., and Coauthors, 2015: Improved seasonal prediction of temperature and precipitation over land in a high-resolution GFDL climate model. *J. Climate*, **28**, 2044–2062, doi:10.1175/JCLI-D-14-00112.1.

Kalnay, E., and Coauthors, 1996: The NCEP/NCAR 40-Year Reanalysis Project. *Bull. Amer. Meteor. Soc.*, **77**, 437–471, doi:10.1175/1520-0477(1996)077<0437:TNYRP>2.0.CO;2.

Kennedy, J. J., N. A. Rayner, R. O. Smith, D. E. Parker, and M. Saunby, 2011: Reassessing biases and other uncertainties in sea surface temperature observations measured in situ since 1850: 2. Biases and homogenization. *J. Geophys. Res.*, **116**, D14104, doi:10.1029/2010JD015220.

Khudeev, R., 2005: A new flood-fill algorithm for closed contour. *Proc. IEEE Int. Siberian Conf. on Control and Communications*, Tomsk, Russia, Institute of Electrical and Electronics Engineers, 172–176, doi:10.1109/SIBCON.2005.1611214.

Klotzback, P. J., 2007: Recent developments in statistical prediction of seasonal Atlantic basin tropical cyclone activity. *Tellus*, **59A**, 511–518, doi:10.3402/tellusa.v59i4.15016.

Knapp, K. R., M. C. Kruk, D. H. Levinson, H. J. Diamond, and C. J. Neumann, 2010: The International Best Track Archive for Climate Stewardship (IBTrACS). *Bull. Amer. Meteor. Soc.*, **91**, 363–376, doi:10.1175/2009BAMS2755.1.

Kobayashi, S., and Coauthors, 2015: The JRA-55 reanalysis: General specifications and basic characteristics. *J. Meteor. Soc. Japan*, **93**, 5–48, doi:10.2151/jmsj.2015-001.

Larson, S. M., and B. P. Kirtman, 2013: The Pacific meridional mode as a trigger for ENSO in a high-resolution coupled model. *Geophys. Res. Lett.*, **40**, 3189–3194, doi:10.1002/grl.50571.

——, and ——, 2014: The Pacific meridional mode as an ENSO precursor and predictor in the North American multimodel ensemble. *J. Climate*, **27**, 7018–7032, doi:10.1175/JCLI-D-14-00055.1.

Lee, H. S., T. Yamashita, and T. Mishima, 2012: Multi-decadal variations of ENSO, the Pacific decadal oscillation and tropical cyclones in the western North Pacific. *Prog. Oceanogr.*, **105**, 67–80, doi:10.1016/j.pocean.2012.04.009.

Li, C., and H. Ma, 2011: Coupled modes of rainfall over China and the Pacific sea surface temperature in boreal summertime. *Adv. Atmos. Sci.*, **28**, 1201–1214, doi:10.1007/s00376-011-0127-3.

——, L. Wu, and P. Chang, 2011: A far-reaching footprint of the tropical Pacific meridional mode on the summer rainfall over the Yellow River Loop Valley. *J. Climate*, **24**, 2585–2598, doi:10.1175/2010JCLI3844.1.

Li, R. C. Y., and W. Zhou, 2014: Interdecadal change in South China Sea tropical cyclone frequency in association with zonal sea surface temperature gradient. *J. Climate*, **27**, 5468–5480, doi:10.1175/JCLI-D-13-00744.1.

Li, X., S. Yang, H. Wang, X. Jia, and A. Kumar, 2013: A dynamical-statistical forecast model for the annual frequency of western Pacific tropical cyclones based on the NCEP Climate Forecast System version 2. *J. Geophys. Res. Atmos.*, **118**, 12 061–12 074, doi:10.1002/2013JD020708.

Lin, C.-Y., J.-Y. Yu, and H.-H. Hsu, 2015: CMIP5 model simulations of the Pacific meridional mode and its connection to the two types of ENSO. *Int. J. Climatol.*, **35**, 2352–2358, doi:10.1002/joc.4130.

Lin, I.-I., I.-F. Pun, and C.-C. Lien, 2014: ''Category-6'' Supertyphoon Haiyan in global warming hiatus: Contribution from subsurface ocean warming. *Geophys. Res. Lett.*, **41**, 8547–8553, doi:10.1002/2014GL061281.

Linkin, M. E., and S. Nigam, 2008: The North Pacific Oscillation–west Pacific teleconnection pattern: Mature-phase structure and winter impacts. *J. Climate*, **21**, 1979–1997, doi:10.1175/2007JCLI2048.1.

Liu, K. S., and J. C. L. Chan, 2003: Climatological characteristics and seasonal forecasting of tropical cyclones making landfall along the south China coast. *Mon. Wea. Rev.*, **131**, 1650–1662, doi:10.1175//2554.1.

——, and ——, 2013: Inactive period of western North Pacific tropical cyclone activity in 1998–2011. *J. Climate*, **26**, 2614–2630, doi:10.1175/JCLI-D-12-00053.1.

Matsuno, T., 1966: Quasi-geostrophic motions in the equatorial area. *J. Meteor. Soc. Japan*, **44**, 25–43.

Mitchell, C. L., 1932: West Indian hurricanes and other tropical cyclones of the North Atlantic of the North Atlantic Ocean. *Mon. Wea. Rev.*, **60**, 253, doi:10.1175/1520-0493(1932)60<253a:WIHAOT>2.0.CO;2.

Murakami, H., and Coauthors, 2015: Simulation and prediction of category 4 and 5 hurricanes in the high-resolution GFDL HiFLOR coupled climate model. *J. Climate*, **28**, 9058–9079, doi:10.1175/JCLI-D-15-0216.1.

Patricola, C. M., R. Saravanan, and P. Chang, 2014: The impact of the El Niño–Southern Oscillation and Atlantic meridional mode on seasonal Atlantic tropical cyclone activity. *J. Climate*, **27**, 5311–5328, doi:10.1175/JCLI-D-13-00687.1.

Pielke, R., Jr., J. Gratz, C. Landsea, D. Collins, M. Saunders, and R. Musulin, 2008: Normalized hurricane damage in the United States: 1900–2005. *Nat. Hazards Rev.*, **9**, 29–42, doi:10.1061/(ASCE)1527-6988(2008)9:1(29).

Rappaport, E. N., 2000: Loss of life in the United States associated with recent Atlantic tropical cyclones. *Bull. Amer. Meteor. Soc.*, **81**, 2065–2073, doi:10.1175/1520-0477(2000)081<2065:LOLITU>2.3.CO;2.

Rienecker, M. M., and Coauthors, 2011: MERRA: NASA's Modern-Era Retrospective Analysis for Research and Applications. *J. Climate*, **24**, 3624–3648, doi:10.1175/JCLI-D-11-00015.1.

Rogers, J. C., 1981: The North Pacific Oscillation. *Int. J. Climatol.*, **1**, 39–57, doi:10.1002/joc.3370010106.

Simpson, J., J. B. Halverson, B. S. Ferrier, W. A. Petersen, R. H. Simpson, R. Blakeslee, and S. L. Durden, 1998: On the role of ''hot towers'' in tropical cyclone formation. *Meteor. Atmos. Phys.*, **67**, 15–35, doi:10.1007/BF01277500.

Sippel, J. A., and F. Zhang, 2008: A probabilistic analysis of the dynamics and predictability of tropical cyclogenesis. *J. Atmos. Sci.*, **65**, 3440–3459, doi:10.1175/2008JAS2597.1.

Smirnov, D., and D. J. Vimont, 2011: Variability of the Atlantic meridional mode during the Atlantic hurricane season. *J. Climate*, **24**, 1409–1424, doi:10.1175/2010JCLI3549.1.

Vecchi, G. A., and Coauthors, 2014: On the seasonal forecasting of regional tropical cyclone activity. *J. Climate*, **27**, 7994–8016, doi:10.1175/JCLI-D-14-00158.1.

Vimont, D. J., and J. P. Kossin, 2007: The Atlantic meridional mode and hurricane activity. *Geophys. Res. Lett.*, **34**, L07709, doi:10.1029/2007GL029683.

——, D. S. Battisti, and A. C. Hirst, 2001: Footprinting: A seasonal connection between the tropics and mid-latitudes. *Geophys. Res. Lett.*, **28**, 3923–3926, doi:10.1029/2001GL013435.

——, J. M. Wallace, and D. S. Battisti, 2003: The seasonal footprinting mechanism in the Pacific: Implications for ENSO. *J. Climate*, **16**, 2668–2675, doi:10.1175/1520-0442(2003)016<2668:TSFMIT>2.0.CO;2.

Vitart, F., and T. N. Stockdale, 2001: Seasonal forecasting of tropical storms using coupled GCM integrations. *Mon. Wea. Rev.*, **129**, 2521–2537, doi:10.1175/1520-0493(2001)129<2521:SFOTSU>2.0.CO;2.

Wang, B., and J. C. L. Chan, 2002: How strong ENSO events affect tropical storm activity over the western North Pacific. *J. Climate*, **15**, 1643–1658, doi:10.1175/1520-0442(2002)015<1643:HSEEAT>2.0.CO;2.

——, R. Wu, and X. Fu, 2000: Pacific–East Asian teleconnection: How does ENSO affect East Asian climate? *J. Climate*, **13**, 1517–1536, doi:10.1175/1520-0442(2000)013<1517:PEATHD>2.0.CO;2.

Wang, C., C. Li, M. Mu, and W. Duan, 2013: Seasonal modulations of different impacts of two types of ENSO events on tropical cyclone activity in the western North Pacific. *Climate Dyn.*, **40**, 2887–2902, doi:10.1007/s00382-012-1434-9.

Wu, G., and N.-C. Lau, 1992: A GCM simulation of the relationship between tropical-storm formation and ENSO. *Mon. Wea. Rev.*, **120**, 958–977, doi:10.1175/1520-0493(1992)120<0958:AGSOTR>2.0.CO;2.

Xie, S.-P., K. Hu, J. Hafner, H. Tokinaga, Y. Du, G. Huang, and T. Sampe, 2009: Indian Ocean capacitor effect on Indo–western Pacific climate during the summer following El Niño. *J. Climate*, **22**, 730–747, doi:10.1175/2008JCLI2544.1.

Yang, X., and Coauthors, 2015: Seasonal predictability of extratropical storm tracks in GFDL's high-resolution climate prediction model. *J. Climate*, **28**, 3592–3611, doi:10.1175/JCLI-D-14-00517.1.

Zhan, R., Y. Wang, and X. Lei, 2011: Contributions of ENSO and east Indian Ocean SSTA to the interannual variability of northwest Pacific tropical cyclone frequency. *J. Climate*, **24**, 509–521, doi:10.1175/2010JCLI3808.1.

——, ——, and M. Wen, 2013: The SST gradient between the southwestern Pacific and the western Pacific warm pool: A new factor controlling the northwestern Pacific tropical cyclone genesis frequency. *J. Climate*, **26**, 2408–2415, doi:10.1175/JCLI-D-12-00798.1.

——, ——, and L. Tao, 2014: Intensified impact of east Indian Ocean SST anomaly on tropical cyclone genesis frequency over the western North Pacific. *J. Climate*, **27**, 8724–8739, doi:10.1175/JCLI-D-14-00119.1.

Zhang, L., P. Chang, and L. Ji, 2009: Linking the Pacific meridional mode to ENSO: Coupled model analysis. *J. Climate*, **22**, 3488–3505, doi:10.1175/2008JCLI2473.1.

Zhang, Q., Q. Liu, and L. Wu, 2009: Tropical cyclone damages in China 1983–2006. *Bull. Amer. Meteor. Soc.*, **90**, 489–495, doi:10.1175/2008BAMS2631.1.

Zhang, W., H. F. Graf, Y. Leung, and M. Herzog, 2012: Different El Niño types and tropical cyclone landfall in East Asia. *J. Climate*, **25**, 6510–6523, doi:10.1175/JCLI-D-11-00488.1.

——, Y. Leung, and J. Min, 2013: North Pacific Gyre Oscillation and the occurrence of western North Pacific tropical cyclones. *Geophys. Res. Lett.*, **40**, 5205–5211, doi:10.1002/grl.50955.